

Appendix C

Hazard Analysis

**CONSEQUENCE ANALYSIS
FOR
CHEVRON HYDROGEN PLANT**

Prepared For

**Environmental Audit, Inc.
1000-A Ortega Way
Placentia, California 92670-7125**

Prepared By

**Quest Consultants Inc.®
908 26th Avenue N.W.
Norman, Oklahoma 73069
Telephone: 405-329-7475
Fax: 405-329-7734**

**03-04-6477
April 21, 2003**

CONSEQUENCE ANALYSIS FOR CHEVRON HYDROGEN PLANT

Introduction

Quest Consultants Inc. has performed a series of release, vapor dispersion, and fire radiation calculations in an effort to quantify the consequences following a release from various process lines on the premises of Chevron's proposed Hydrogen Plant in the El Segundo Refinery. The releases were designed to simulate what would happen if one of several lines containing either anhydrous ammonia (AnNH₃), aqueous ammonia (AqNH₃), natural/fuel gas, hydrogen (H₂), or pentanes was to fully fail and the material contained therein was released to the environment.

Site-Specific Information

Several of the parameters defined in the analysis are:

Toxic Material Pipelines

Parameters	Current AnNH ₃	Proposed AnNH ₃ Feed to Hydrogen Plant	Proposed AqNH ₃ to New Hydrogen Plant
Pipeline diameter	2-inch	2-inch	2-inch
Material composition	Anhydrous ammonia	Anhydrous ammonia	Aqueous ammonia (30% by weight in water)
Temperature	87°F	87°F	87°F
Pressure	170 psig	170 psig	180 psig
Average flow rate	13 gpm	13 gpm	216 gpd
Approximate length of pipeline	5,000 ft	1,100 ft	750 ft

Fuel Gas and Pentanes Pipelines

Parameters	Proposed Natural Gas Line	Proposed Fuel Gas Line	Proposed Pentanes Line
Pipeline diameter	10-inch	6-inch	3-inch
Material composition	Natural gas	Fuel gas	Pentanes
Temperature	60°F	65°F	70°F
Pressure	130 psig	85 psig	150 psig
Average flow rate	21 mmscfd	10 mmscfd	42,000 lb/hr
Approximate length of pipeline	6,000 ft	650 ft	630 ft

Hydrogen Pipelines

Parameters	Existing Steam Methane Reformer (SMR) Product H ₂ Pipeline	Proposed H ₂ Plant Pipeline 1	Proposed H ₂ Plant Pipeline 2
Pipeline diameter	8-inch	8-inch	8-inch
Material composition	95.7%* mol H ₂	99% mol H ₂	99% mol H ₂
Temperature	70°F	104°F	100°F
Pressure	835 psig	391 psig	935 psig
Average flow rate	88.55 MMSCFD	90 MMSCFD	90 MMSCFD
Approximate length of pipeline	420 ft	400 ft	910 ft

* Remainder is primarily methane

Atmospheric Conditions

Wind speed = 1.5 m/s and 5 m/s

Relative humidity = 70%

Air temperature = 77°F

Atmospheric stability = Pasquill-Gifford F (extremely stable) and Pasquill-Gifford D (neutral)

[Atmospheric stability is classified by the letters A through F. In general, the most unstable atmosphere is characterized by stability class A. Stability A would correspond to an atmospheric condition where there is strong solar radiation and moderate winds. This combination of radiation and winds allows for rapid fluctuations in the air and thus greater mixing of the released gas with time. Stability D is characterized by fully overcast or partial cloud cover during both daytime and nighttime. The atmospheric turbulence is not as great during D conditions as during A conditions; thus, the gas will not mix as quickly with the surrounding atmosphere. Stability F corresponds to the most “stable” atmospheric conditions. Stability F generally occurs during the early morning hours before sunrise (thus, no solar radiation) and under low winds. The combination of low winds and lack of solar heating allows for the atmosphere to appear calm or still and thus restricts the ability to actively mix with the released gas.]

Toxic Gas Hazards

Release/dispersion calculations were made in order to determine the extent of downwind travel of the ammonia gas released as a jet in the anhydrous ammonia case or evolving from the aqueous ammonia pool formed in the case of the aqueous ammonia release. Dispersion calculations were performed until a specific ammonia concentration was reached in the downwind direction. The ammonia gas concentration chosen for evaluation was:

ERPG-2 for Ammonia = 200 ppm

Emergency Response Planning Guideline (ERPG) Level 2. The maximum airborne concentration below which it is believed nearly all individuals could be exposed for up to one hour without experiencing or developing irreversible or other serious health effects or symptoms that could impair their ability to take protective action.

Flammable Gas Hazards

Release/dispersion calculations were made in order to determine the downwind travel of the flash fire hazard as defined by the flammable cloud following the release of natural gas, fuel gas, pentanes, and hydrogen. The dispersion calculations were performed until the lower flammable limit (LFL) concentration was reached. For the natural gas and fuel gas jet dispersion calculations, this concentration was 5% on a molar (or volume) basis (5% is the lower flammable limit, or LFL, for methane, the primary component in the gas streams). For all of the hydrogen lines, this concentration was approximately 4% on a molar (or volume) basis (the LFL for the hydrogen-methane mixtures). For the evaporating pool of pentanes, this concentration was taken to be 1.5% on a molar (or volume) basis (the LFL for *n*-pentane).

Fire Radiation Hazards

Torch and pool fire radiation calculations were made to determine the distances from the release that could be affected by an ignited pipeline release. The radiation level evaluated in this study was 1,600 Btu/(hr@²). Exposure of bare skin to thermal radiation with an intensity of 1,600 Btu/(hr@²) is sufficient to cause second-degree burns after 30 seconds of exposure¹.

Consequence Analysis

When performing site-specific consequence analysis studies, the ability to accurately model the release, dilution, and dispersion of gases and aerosols is important if an accurate assessment of potential exposure is to be attained. For this reason, Quest uses a modeling package, CANARY by Quest®, that contains a set of complex models that calculate release conditions, initial dilution of the vapor (dependent upon the release characteristics), and the subsequent dispersion of the vapor introduced into the atmosphere. The models contain algorithms that account for thermodynamics, mixture behavior, transient release rates, gas cloud density relative to air, initial velocity of the released gas, and heat transfer effects from the surrounding atmosphere and the substrate. The release and dispersion models contained in the QuestFOCUS package (the predecessor to CANARY by Quest) were reviewed in a United States Environmental Protection Agency (EPA) sponsored study² and an American Petroleum Institute (API) study³. In both studies, the QuestFOCUS software was evaluated on technical merit (appropriateness of models for specific applications) and on model predictions for specific releases. One conclusion drawn by both studies was that the dispersion software tended to over-predict the extent of the gas cloud travel, thus resulting in too large a cloud when compared to the test data (i.e., a conservative approach).

¹“Relationship Between Pain and Tissue Damage Due to Thermal Radiation,” A. M. Stoll and L. C. Greene. *Journal of Applied Physiology*, No. 14, 1959: pp. 373-382.

²*Evaluation of Dense Gas Dispersion Models*. Prepared for the U.S. Environmental Protection Agency by TRC Environmental Consultants Inc., East Hartford, Connecticut, 06108, EPA Contract No. 68-02-4399, May, 1991.

³*Hazard Response Modeling Uncertainty (A Quantitative Method); Volume II, Evaluation of Commonly-Used Hazardous Gas Dispersion Models*, S. R. Hanna, D. G. Strimaitis, and J. C. Chang, Study cosponsored by the Air Force Engineering and Services Center, Tyndall Air Force Base, Florida, and the American Petroleum Institute, and performed by Sigma Research Corporation, Westford, Massachusetts, September 1991.

A study prepared for the Minerals Management Service⁴ reviewed models for use in modeling routine and accidental releases of flammable and toxic gases. CANARY by Quest received the highest possible ranking in the science and credibility areas. In addition, the report recommends CANARY by Quest for use when evaluating toxic and flammable gas releases. The specific models contained in the CANARY by Quest software package have also been extensively reviewed.

CANARY also contains models for pool fire and torch fire radiation. These models account for impoundment configuration, material composition, target height relative to the flame, target distance from the flame, atmospheric attenuation (includes humidity), wind speed, and atmospheric temperature. Both are based on information in the public domain (published literature) and have been validated with experimental data.

Technical descriptions of the CANARY models used in this study are presented in Appendix A.

Anhydrous Ammonia, Natural Gas, Fuel Gas, Pentanes, and Hydrogen Dispersion Results

CANARY by Quest was used to model the momentum jet releases resulting from failures of anhydrous ammonia, natural gas, fuel gas, and hydrogen lines, as well as the heavy gas dispersion resulting from evaporation of the liquid pool following failure of the pentanes line. CANARY by Quest was also used to model the fire radiation hazard posed by torch fires resulting from failures of natural gas, fuel gas, and hydrogen lines, as well as the pool fire resulting from failure of the pentanes line. The results of these calculations are presented in Tables 1, 2, and 3.

**Table 1
Toxic Vapor Dispersion Results**

Release Scenario	Wind Speed (m/s)	Stability Class	Ammonia Concentration ERPG-2 (ppm)	Distance to ERPG-2 (ft)
Current anhydrous ammonia line	1.5	F	200	3,050
	5.0	D	200	2,110
Proposed anhydrous ammonia feed line to AirLiquide	1.5	F	200	2,040
	5.0	D	200	1,710
Proposed aqueous ammonia line to AirLiquide	1.5	F	200	65
	5.0	D	200	50

⁴A Critical Review of Four Types of Air Quality Models Pertinent to MMS Regulatory and Environmental Assessment Missions, Joseph C. Chang, Mark E. Fernau, Joseph S. Scire, and David G. Strimaitis. Mineral Management Service, Gulf of Mexico OCS Region, U.S. Department of the Interior, New Orleans, November, 1998.

Table 2
Flammable Vapor Dispersion Results

Release Scenario	Wind Speed (m/s)	Stability Class	Flammable Gas Concentration LFL (mole %)	Distance to LFL (ft)
Proposed natural gas line	1.5	F	5	85
	5.0	D	5	30
Proposed fuel gas line	1.5	F	5	55
	5.0	D	5	20
Proposed pentanes line	1.5	F	1.5	60
	5.0	D	1.5	10
Existing SMR product H ₂	1.5	F	4	100
	5.0	D	4	55
New H ₂ plant pipeline 1	1.5	F	4	90
	5.0	D	4	55
New H ₂ plant pipeline 2	1.5	F	4	95
	5.0	D	4	60

Table 3
Fire Radiation Results

Release Scenario	Wind Speed (m/s)	Stability Class	Fire Radiation Level (Btu/(hr@ ²))	Distance to Radiant Level (ft)
Proposed natural gas line (torch fire)	1.5	F	1,600	120
	5.0	D	1,600	115
Proposed fuel gas line (torch fire)	1.5	F	1,600	75
	5.0	D	1,600	70
Proposed pentanes line (pool fire)	1.5	F	1,600	50
	5.0	D	1,600	55
Existing SMR product H ₂ pipeline (torch fire)	1.5	F	1,600	90
	5.0	D	1,600	95
New H ₂ plant pipeline 1 (torch fire)	1.5	F	1,600	85
	5.0	D	1,600	90
New H ₂ plant pipeline 2 (torch fire)	1.5	F	1,600	95
	5.0	D	1,600	100

Vaporization of Ammonia Gas from an Aqueous Ammonia Pool

The hazard zones resulting from liquid releases of aqueous ammonia (30% ammonia by weight) onto the ground were evaluated to determine the downwind extent of the gas cloud containing 200 ppm NH₃. The Mackay and Matsugu model⁵ is the basis of many of the current pool vaporization models published today. This model has been partially validated using the authors' experimental data.

The equation used to compute evaporation rates is shown in Equation 1.

$$N = k_m A(P - P_\infty) / RT \quad (1)$$

where: N = evaporation rate, g-moles/hr
 k_m = mass transfer coefficient, m/hr
 A = area of pool, m²
 P = partial pressure or vapor pressure of liquid, atm
 P_∞ = background pressure of evaporating liquid, atm
 R = gas constant, atm-m³/g-mole-K, 82.06 x 10⁻⁶
 T = temperature, K

The equation given by Mackay and Matsugu⁵ to compute the mass transfer coefficient is:

$$k_m = 0.0292 S_c^{2/3} U^{0.78} \rho^{-0.11} \quad (2)$$

where: U = wind speed at a height of 10 m, m/hr
 S_c = Schmidt Number, $\mu / \rho D$
 μ = air viscosity, kg/m·hr
 ρ = air density, kg/m³
 D = evaporating liquid diffusivity, m²/hr

For these calculations, the following parameters were used.

Liquid pool temperature = 77EF
Partial pressure of ammonia above liquid pool (at 77EF) = 5.1 psia

As can be seen from Equation 1, as the liquid pool diameter increases, the total evaporation rate also increases. The extent of the liquid pool was determined using CANARY by Quest and the consequent evolution rate of ammonia from the pool was calculated using the method described above.

Dispersion of Ammonia Gas from an Aqueous Ammonia Pool

The pool vaporization model provides one of the inputs to a dispersion model. The ammonia gas evolving from the pool can be treated as a neutrally buoyant gas. The ammonia/air mixture over the liquid pool surface is slowly swept from the pool surface by the ambient wind field. Since the ammonia/air mixture would not exhibit any dense gas effects (the molecular weight of the mixture is less than air), a form of a Gaussian dispersion model would be appropriate. In this report, an area source Gaussian model was used in which the

⁵“Evaporation Rates of Liquid Hydrocarbon Spills on Land and Water,” Donald Mackay and Ronald S. Matsugu. *The Canadian Journal of Chemical Engineering*, Vol. 51, August, 1973: pp. 434-439.

area source is approximated by a series of line sources. The line source model is taken from Dobbins⁶. For this analysis, urban dispersion coefficients⁷ were used. Results of these calculations are given in Table 1.

For the aqueous ammonia release scenario, the distance listed in Table 1 would not vary as long as the liquid pool remained. In essence, the plume reaches steady state within minutes of the release, and will maintain its shape until the weather conditions change or the liquid pool is eliminated.

Conclusions

Table 4 presents the maximum downwind extent of each hazard zone that is applicable to each release considered in this study, but it provides no information on the areal extent, or outline, of each hazard zone. Such information can be illustrated by the use of a hazard footprint, which is defined as the area over which a given unique accident is capable of producing some level of undesirable consequences. The hatched area in Figure 1 is an example of a hazard footprint for the proposed anhydrous ammonia pipeline.

**Table 4
Maximum Hazard Zone Summary**

Pipeline	Existing/Proposed	Maximum Extent of Hazard (ft)		
		200 ppm NH ₃	LFL	1,600 Btu/(hr@ ²)
Anhydrous NH ₃	Existing	3,050	N/A	N/A
Anhydrous NH ₃	Proposed	2,040	N/A	N/A
Aqueous NH ₃	Proposed	65	N/A	N/A
Natural gas	Proposed	N/A	85	120
Fuel gas	Proposed	N/A	55	75
Pentanes	Proposed	N/A	60	55
SMR product H ₂	Existing	N/A	100	95
H ₂ plant pipeline 1	Proposed	N/A	90	90
H ₂ plant pipeline 2	Proposed	N/A	95	100

Rotating a hazard footprint around its point of origin produces a circle, which is known as a vulnerability zone. Any point within that circle could, under some set of circumstances, be exposed to a hazard level that equals or exceeds the endpoint used to define the hazard footprint. Except for accidents that produce circular hazard footprints (e.g., a Boiling Liquid Expanding Vapor explosion [BLEVE]), the whole area within a vulnerability zone cannot be simultaneously affected by the effects of a unique accident. An example of a hazard footprint and its associated vulnerability zone for the proposed anhydrous ammonia pipeline is shown in Figure 1.

⁶*Atmospheric Motion and Air Pollution*, Richard A. Dobbins. John Wiley & Sons, Inc., 1979.

⁷*Diffusion Estimation for Small Emissions*, G. A. Briggs. ATDL Report No. 79, ATDL, Post Office Box E, Oak Ridge, Tennessee 37830, 1973.

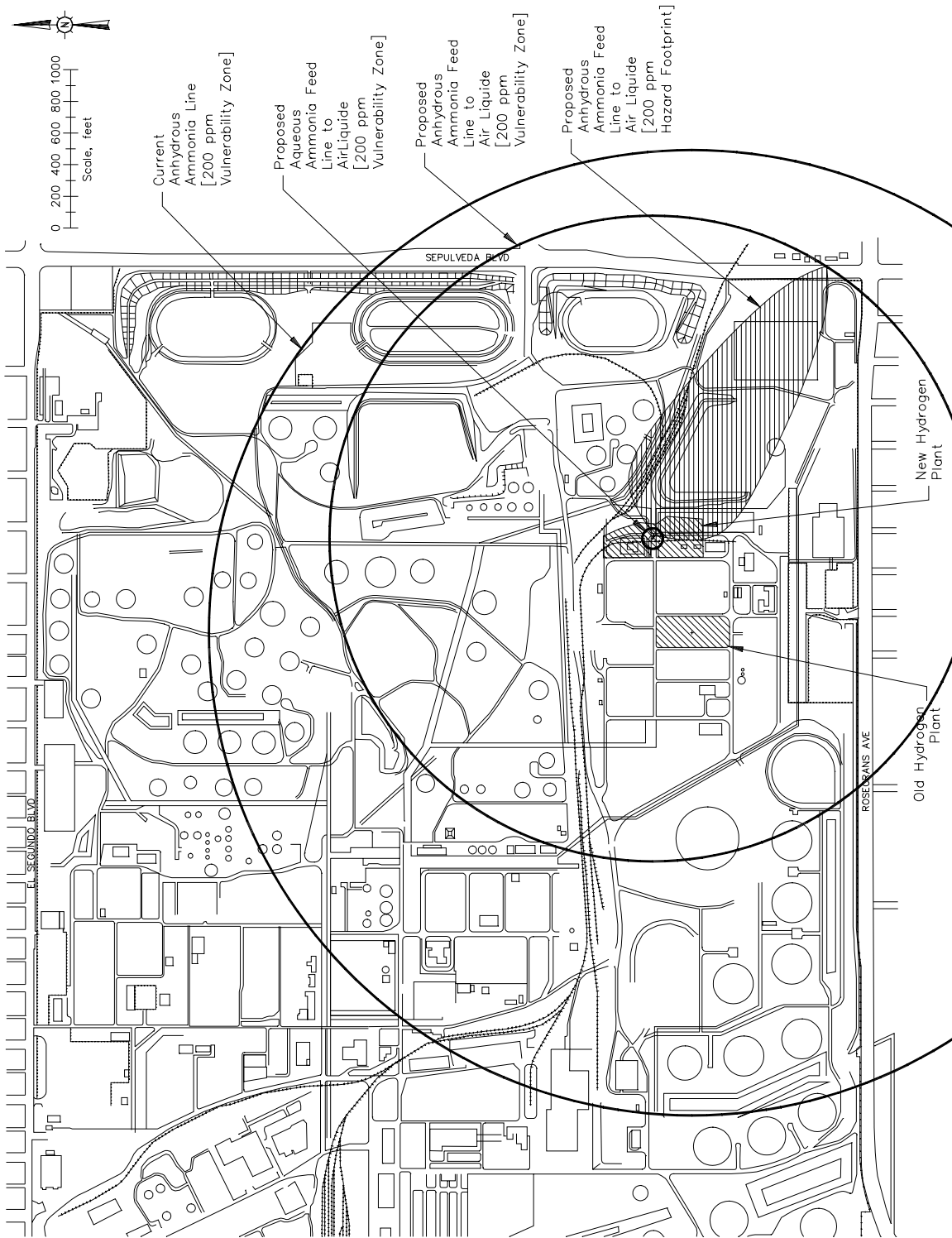


Figure 1
Toxic Pipelines Vulnerability Zones

Vulnerability zones can be used to define the size of the area around a release within which there is a finite probability of exposure to a defined hazard. Persons located outside this area would not be exposed to the hazard.

Vulnerability zones for the largest hazards at a release point along each flammable pipeline route are depicted in Figure 2.

The results of this study can be summarized as;

1. The largest potential hazard is posed by a failure of the existing anhydrous ammonia line.
2. Addition of the new, shorter anhydrous ammonia line will present a smaller hazard than the existing line.
3. The new aqueous ammonia line will present a significantly smaller hazard than either the existing or proposed anhydrous ammonia line.
4. Torch fire radiation presents a larger hazard zone than does the flash fire for both the natural gas and fuel gas lines.
5. The flash fire hazard zone for the pentanes line is larger than the pool fire radiation hazard zone.
6. The flash fire and torch fire radiation hazard zones for the hydrogen lines are all of similar magnitude.

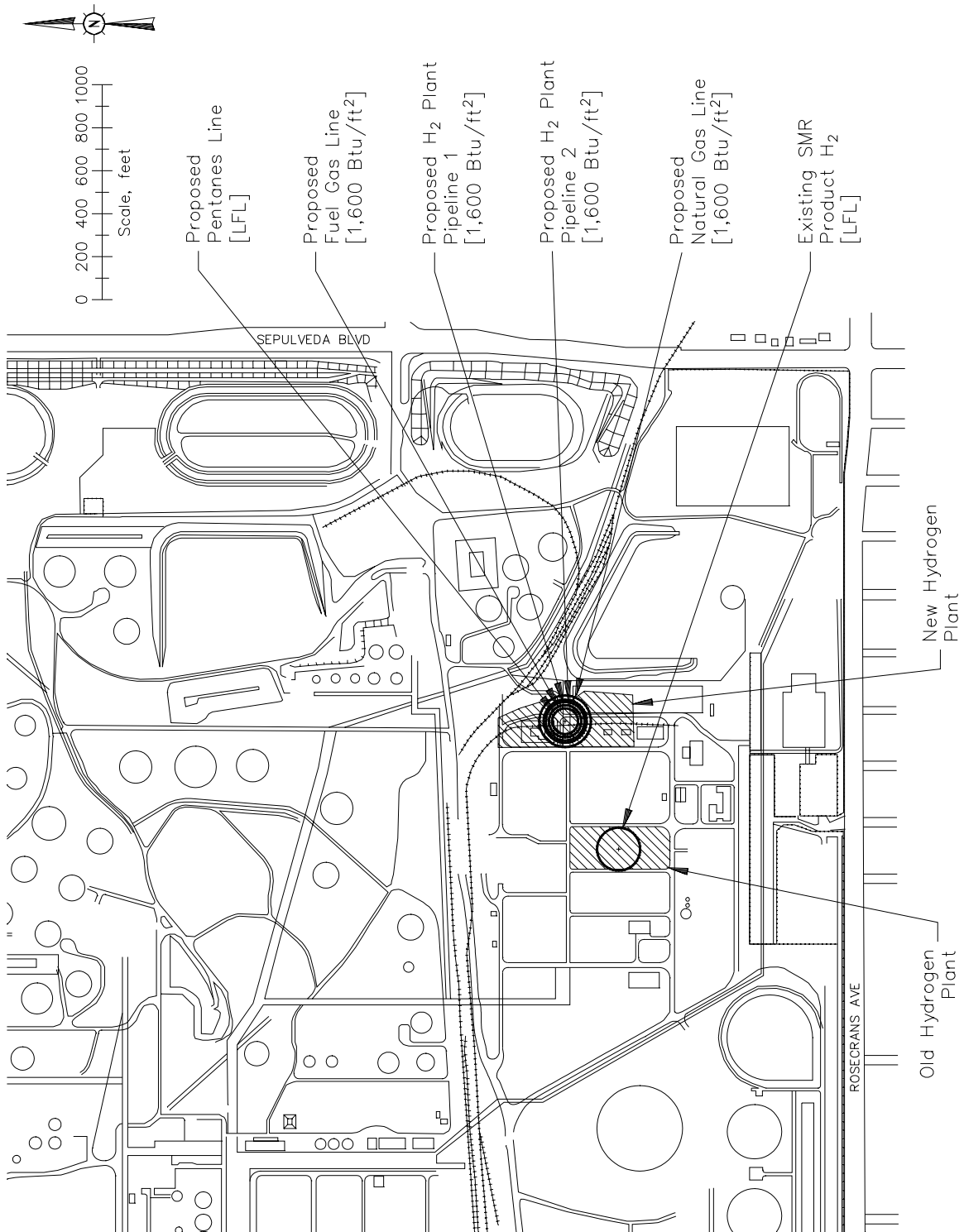


Figure 2
Flammable Pipelines Vulnerability Zones

APPENDIX A

CANARY BY QUEST® MODEL DESCRIPTIONS

The following model descriptions are taken from the CANARY by Quest User Manual.

Section A	Engineering Properties
Section B	Pool Fire Radiation Model
Section C	Torch Fire and Flare Radiation Model
Section E	Fluid Release Model
Section F	Momentum Jet Dispersion Model
Section G	Heavy Gas Dispersion Model

Engineering Properties

Purpose

The purpose of this model is to provide an accurate means of computing physical and thermodynamic properties of a wide range of chemical mixtures and pure components using a minimum of initial information.

Required Data

- (a) Fluid composition
- (b) Temperature and pressure of the fluid prior to release

Methodology

Basic thermodynamic properties are computed using the Peng-Robinson equation of state [Peng and Robinson, 1976]. The necessary physical and thermodynamic properties are calculated in the following manner.

- Step 1: The temperature and pressure of the fluid at storage conditions and the identity and mole fraction of each component of the fluid are obtained. Mixture parameters are determined using data from the extensive properties data base within CANARY.
- Step 2: Each calculation begins with the computation of the vapor and liquid fluid composition. For cases where the temperature and pressure result in only one phase being present, the vapor or liquid composition will be the same as the initial feed composition. The composition calculation is an iterative procedure using a modification of the techniques described by Starling [1973].
- Step 3: Once the vapor and liquid compositions are known, the vapor and liquid densities, enthalpies, entropies, and heat capacities can be computed directly. Other physical properties (viscosity, thermal conductivity, surface tension, etc.) are computed using correlations developed in Reid, Prausnitz, and Poling [1987].
- Step 4: A matrix of properties is computed over a range of temperatures and pressures. Physical and thermodynamics properties required by other models within CANARY are then interpolated from this table.

Basic Thermodynamic Equations

$$Z^3 - (1 - B) \cdot Z^2 + (A - 3 \cdot B^2 - 2 \cdot B) \cdot Z - (A \cdot B - B^2 - B^3) = 0 \quad (1)$$

where: Z = fluid compressibility factor, $\frac{P \cdot V}{R \cdot T}$, dimensionless

P = system pressure, kPa

V = fluid specific volume, m³/kmol

R = gas constant, $8.314 \text{ m}^3\text{Pa}/(\text{kmol}\cdot\text{K})$

T = absolute temperature, K

$$A = \frac{a \cdot P}{R^2 \cdot T^2}$$

$$a = 0.45724 \cdot \frac{R^2 \cdot T^2}{P_c} \cdot \alpha$$

$$\alpha = \left[1 + m \cdot (1 - T_r^{0.5})^2 \right]$$

$$m = 0.37464 + 1.54226 \cdot \omega - 0.26992 \cdot \omega^2$$

ω = acentric factor

$$T_r = \frac{T}{T_c}$$

T_c = pseudo-critical temperature, K

P_c = pseudo-critical pressure, kPa

$$B = \frac{b \cdot P}{R \cdot T}$$

$$b = 0.0778 \cdot R \cdot \frac{T_c}{P_c}$$

$$H = H^o + \frac{P}{\rho} - R \cdot T + \int_0^P \left[P - T \cdot \left(\frac{\partial P}{\partial T} \right)_\rho \right] \cdot \left(\frac{d\rho}{\rho^2} \right) \quad (2)$$

where: H = enthalpy of fluid at system conditions, kJ/kg

H^o = enthalpy of ideal gas at system temperature, kJ/kg

$$S = S^o - R \cdot \ln(\rho \cdot R \cdot T) + \int_0^P \left[\rho \cdot R - \left(\frac{\partial P}{\partial T} \right)_\rho \right] \cdot \left(\frac{d\rho}{\rho^2} \right) \quad (3)$$

where: S = entropy of fluid at system conditions, kJ/(kg·K)

S^o = entropy of ideal gas at system temperature, kJ/(kg·K)

$$R \cdot T \cdot \ln \left(\frac{f_i}{f_i^o} \right) = \left[(H_i - H_i^o) - T \cdot (S_i - S_i^o) \right] \quad (4)$$

where: f_i = fugacity of component i , kPa

f_i^o = standard state reference fugacity, kPa

References

Peng, D., and D. B. Robinson, "New Two-Constant Equation of State." *Industrial Engineering Chemistry Fundamentals*, Vol. 15, No. 59, 1976.

Reid, R. C., J. M. Prausnitz, and B. E. Poling, *The Properties of Gases and Liquids* (Fourth Edition). McGraw-Hill Book Company, New York, New York, 1987.

Starling, K. E., *Fluid Thermodynamic Properties for Light Petroleum Systems*. Gulf Publishing Company, Houston, Texas, 1973.

Pool Fire Radiation Model

Purpose

The purpose of this model is to predict the impact of fire radiation emitted by flames that are fueled by vapors emanating from liquid pools. Specifically, the model predicts the maximum radiant heat flux incident upon a target as a function of distance between the target and the flame.

Required Data

- (a) Composition of the liquid in the pool
- (b) Temperature of the liquid in the pool
- (c) Wind speed
- (d) Air temperature
- (e) Relative humidity
- (f) Elevation of the target (relative to grade)
- (g) Elevation of the pool (relative to grade)
- (h) Dimensions of the free surface of the pool
- (i) Orientation of the pool (relative to the wind direction)
- (j) Spill surface (land or water)

Methodology

Step 1: The geometric shape of the flame is defined. The flame column above a circular pool, square pool, or rectangular pool is modeled as an elliptical cylinder.

Step 2: The dimensions of the flame column are determined. The dimensions of the base of the flame are defined by the pool dimensions. An empirical correlation developed by Thomas [1965] is used to calculate the length (height) of the flame.

$$L = 42 \cdot D_h \cdot \left(\frac{\dot{m}}{\rho_a \cdot (g \cdot D_h)^{0.5}} \right)^{0.61}$$

where: L = length (height) of the flame, m

D_h = hydraulic diameter of the liquid pool, m

\dot{m} = mass burning flux, kg/(m²Ⓢ)

ρ_a = density of air, kg/m³

g = gravitational acceleration, 9.8 m/s²

Notes: Mass burning fluxes used in the Thomas equation are the steady-state rates for pools on land (soil, concrete, etc.) or water, whichever is specified by the user.

For pool fires with hydraulic diameters greater than 100 m, the flare length, L , is set equal to the length calculated for $D_h = 100$ m.

Step 3: The angle (Φ) to which the flame is bent from vertical by the wind is calculated using an empirical correlation developed by Welker and Sliepcevich [1970].

$$\frac{\tan(\Phi)}{\cos(\Phi)} = 3.2 \cdot \left(\frac{D_h \cdot u \cdot \rho_a}{\mu_a} \right)^{0.07} \cdot \left(\frac{u^2}{g \cdot D_h} \right)^{0.7} \cdot \left(\frac{\rho_v}{\rho_a} \right)^{-0.6}$$

where: Φ = angle the flame tilts from vertical, degrees

u = wind speed, m/s

μ_a = viscosity of air, kg/(m \cdot s)

ρ_v = density of fuel vapor, kg/m 3

Step 4: The increase in the downwind dimension of the base of the flame (flame drag) is calculated using a generalized form of the empirical correlation Moorhouse [1982] developed for large circular pool fires.

$$D_w = 1.5 \cdot D_x \cdot \left(\frac{u^2}{g \cdot D_x} \right)^{0.069}$$

where: D_w = downwind dimension of base of tilted flame, m

D_x = downwind dimension of the pool, m

Step 5: The flame is divided into two zones: a clear zone in which the flame is not obscured by smoke; and a smoky zone in which a fraction of the flame surface is obscured by smoke. The length of the clear zone is calculated by the following equation, which is based on an empirical correlation developed by Pritchard and Binding [1992].

$$L_c = 55.05 \cdot D_h^{-0.6} \cdot \left(\frac{\dot{m}}{\rho_a} \right)^{1.13} \cdot (u+1)^{0.179} \cdot \left(\frac{C}{H} \right)^{-2.49}$$

where: L_c = length of the clear zone, m

$\frac{C}{H}$ = carbon/hydrogen ratio of fuel, dimensionless

Step 6: The surface flux of the clear zone is calculated using the following equation.

$$q_{cz} = q_{sm} \cdot (1 - e^{-b \cdot D_h})$$

where: q_{cz} = surface flux of the clear zone, kW/m 2

q_{sm} = maximum surface flux, kW/m 2

b = extinction coefficient, m $^{-1}$

Average surface flux of the smoky zone, q_{cz} , is then calculated, based on the following assumptions.

- 7 The smoky zone consists of clean-burning areas and areas in which the flame is obscured by smoke.
- 7 Within the smoky zone, the fraction of the flame surface that is obscured by smoke is a function of the fuel properties and pool diameter.
- 7 Smoky areas within the smoky zone have a surface flux of 20 kW/m² [Hagglund and Persson, 1976].
- 7 Clean-burning areas of the smoky zone have the same surface flux as the clean-burning zone.
- 7 The average surface flux of the smoky zone is the area-weighted average of the surface fluxes for the smoky areas and the clean-burning areas within the smoky zone.

(This two-zone concept is based on the Health and Safety Executive POOLFIRE6 model, as described by Rew and Hulbert [1996].)

Step 7: The surface of the flame is divided into numerous differential areas. The following equation is then used to calculate the view factor from a differential target, at a specific location outside the flame, to each differential area on the surface of the flame.

$$F_{dA_t \rightarrow dA_f} = \frac{\cos(\beta_t) \cdot \cos(\beta_f)}{\pi \cdot r^2} \cdot dA_f \quad \text{for } [\beta_t] \text{ and } [\beta_f] < 90^\circ$$

where: $F_{dA_t \rightarrow dA_f}$ = view factor from a differential area on the target to a differential area on the surface of the flame, dimensionless

dA_f = differential area on the flame surface, m²

dA_t = differential area on the target surface, m²

r = distance between differential areas dA_t and dA_f , m

β_t = angle between normal to dA_t and the line from dA_t to dA_f , degrees

β_f = angle between normal to dA_f and the line from dA_t to dA_f , degrees

Step 8: The radiant heat flux incident upon the target is computed by multiplying the view factor for each differential area on the flame by the appropriate surface flux (q_{cz} or q_{sz}) and by the appropriate atmospheric transmittance, then summing these values over the surface of the flame.

$$q_{ai} = \sum_{A_f} q_{sf} \cdot F_{dA_t \rightarrow dA_f} \cdot \tau$$

where: q_{ai} = attenuated radiant heat flux incident upon the target due to radiant heat emitted by the flame, kW/m²

A_f = area of the surface of the flame

q_{sf} = radiant heat flux emitted by the surface of the flame, kW/m² (q_{sf} equals either q_{cz} or q_{sz} , as appropriate)

τ = atmospheric transmittance, dimensionless

Atmospheric transmittance, τ , is a function of absolute humidity and r , the path length between differential areas on the flame and target [Wayne, 1991].

Step 9: Steps 7 and 8 are repeated for numerous target locations.

Validation

Several of the equations used in the Pool Fire Radiation Model are empirical relationships based on data from medium- to large-scale experiments, which ensures reasonably good agreement between model predictions and experimental data for variables such as flame length and tilt angle. Comparisons of experimental data and model predictions for incident heat flux at specific locations are more meaningful and of greater interest. Unfortunately, few reports on medium- or large-scale experiments contain the level of detail required to make such comparisons.

One source of detailed test data is a report by Welker and Cavin [1982]. It contains data from sixty-one pool fire tests involving commercial propane. Variables that were examined during these tests include pool size (2.7 to 152 m²) and wind speed. Figure B-1 compares the predicted values of incident heat flux with experimental data from the sixty-one pool fire tests.

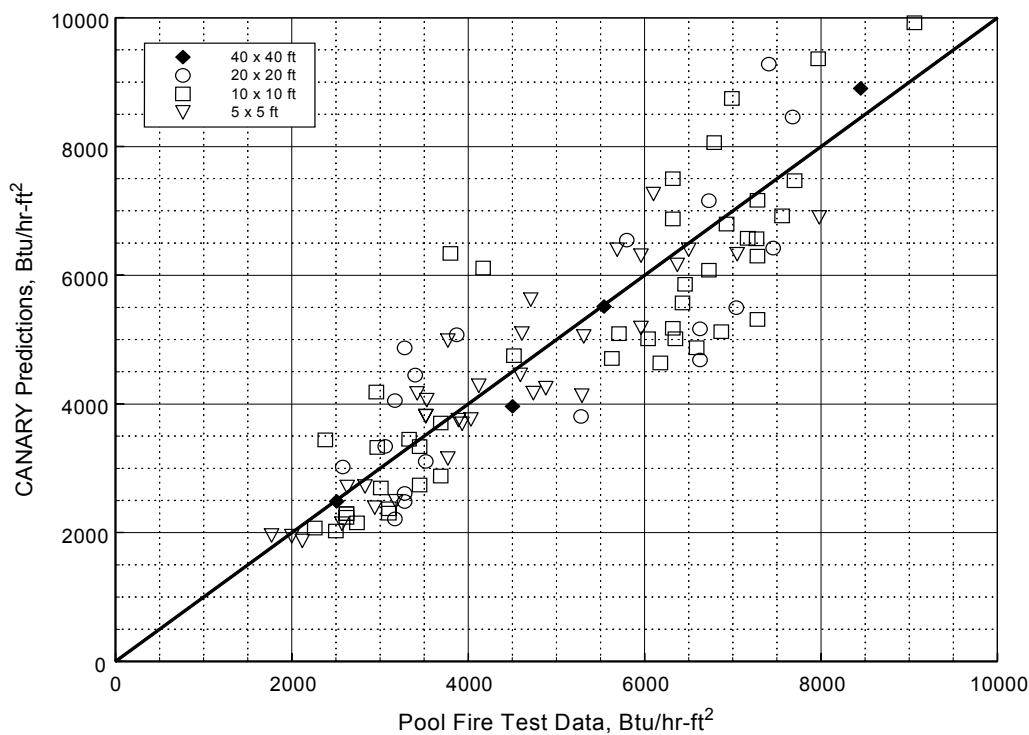


Figure B-1

References

- Hagglund B., and L. Persson, *The Heat Radiation from Petroleum Fires*. FOA Rapport, Forsvarets Forskningsanstalt, Stockholm, Sweden, 1976.
- Moorhouse, J., "Scaling Criteria for Pool Fires Derived from Large-Scale Experiments." *The Assessment of Major Hazards*, Symposium Series No. 71, The Institution of Chemical Engineers, Pergamon Press Ltd., Oxford, United Kingdom, 1982: pp. 165-179.
- Pritchard, M. J., and T. M. Binding, "FIRE2: A New Approach for Predicting Thermal Radiation Levels from Hydrocarbon Pool Fires." *ICHEME Symposium Series*, No. 130, 1992: pp. 491-505.

Rew, P. J., and W. G. Hulbert, *Development of Pool Fire Thermal Radiation Model*. HSE Contract Research Report No. 96/1996.

Thomas, P. H., *F.R. Note 600*, Fire Research Station, Borehamwood, England, 1965.

Wayne, F. D., "An Economical Formula for Calculating Atmospheric Infrared Transmissivities." *Journal of Loss Prevention in the Process Industries*, Vol. 4, January, 1991: pp. 86-92.

Welker, J. R., and W. D. Cavin, *Vaporization, Dispersion, and Radiant Fluxes from LPG Spills*. Final Report No. DOE-EP-0042, Department of Energy Contract No. DOE-AC05-78EV-06020-1, May, 1982 (NTIS No. DOE-EV-06020-1).

Welker, J. R., and C. M. Sliepcevich, *Susceptibility of Potential Target Components to Defeat by Thermal Action*. University of Oklahoma Research Institute, Report No. OURI-1578-FR, Norman, Oklahoma, 1970.

Torch Fire and Flare Radiation Model

Purpose

The purpose of this model is to predict the impact of fire radiation emitted by burning jets of vapor. Specifically, the model predicts the maximum radiant heat flux incident upon a target as a function of distance between the target and the point of release.

Required Data

- (a) Composition of the released material
- (b) Temperature and pressure of the material before release
- (c) Mass flow rate of the material being released
- (d) Diameter of the exit hole
- (e) Wind speed
- (f) Air temperature
- (g) Relative humidity
- (h) Elevation of the target (relative to grade)
- (i) Elevation of the point of release (relative to grade)
- (j) Angle of the release (relative to horizontal)

Methodology

Step 1: A correlation based on a Momentum Jet Model is used to determine the length of the flame. This correlation accounts for the effects of:

- 7 composition of the released material,
- 7 diameter of the exit hole,
- 7 release rate,
- 7 release velocity, and
- 7 wind speed.

Step 2: To determine the behavior of the flame, the model uses a momentum-based approach that considers increasing plume buoyancy along the flame and the bending force of the wind. The following equations are used to determine the path of the centerline of the flame [Cook, et al., 1987].

$$\Phi_x = (\rho_{ja})^{0.5} \cdot \bar{u} \cdot \sin(\theta) \cdot \cos(\varphi) + (\rho_\infty)^{0.5} \cdot u_\infty \quad (\text{downwind})$$

$$\Phi_y = (\rho_{ja})^{0.5} \cdot \bar{u} \cdot \sin(\theta) \cdot \sin(\varphi) \quad (\text{crosswind})$$

$$\Phi_z = (\rho_{ja})^{0.5} \cdot \bar{u} \cdot \cos(\theta) + (\rho_\infty)^{0.5} \cdot u_b \cdot \frac{(i+1)}{n} \quad (\text{vertical})$$

- where: Φ_{XYZ} = momentum flux in X, Y, Z direction
 ρ_{ja} = density of the jet fluid at ambient conditions, kg/m^3
 \bar{u} = average axial velocity of the flame, m/s
 θ = release angle in $X-Z$ plane (relative to horizontal), degrees
 φ = release angle in $X-Y$ plane (relative to downwind), degrees
 ρ_{∞} = density of air, kg/m^3
 u_{∞} = wind speed, m/s
 ρ_b = density of combustion products, kg/m^3
 u_b = buoyancy velocity, m/s
 n = number of points taken along the flame length

These correlations were developed to predict the path of a torch flame when released at various orientations. The model currently does not allow a release angle in a crosswind direction; the release angle is confined to the downwind/vertical plane (i.e., $\varphi = 0$).

- Step 3: The angle of flame tilt is defined as the inclination of a straight line between the point of release and the end point of the flame centerline path (as determined in Step 2).
- Step 4: The geometric shape of the flame is defined as a frustum of a cone (as suggested by several flare/fire researchers [e.g., Kalghatgi, 1983, Chamberlain, 1987]), but modified by adding a hemisphere to the large end of the frustum. The small end of the frustum is positioned at the point of release, and the centerline of the frustum is inclined at the angle determined in Step 3.
- Step 5: The surface emissive power is determined from the molecular weight and heat of combustion of the burning material, the release rate and velocity, and the surface area of the flame.
- Step 6: The surface of the flame is divided into numerous differential areas. The following equation is then used to calculate the view factor from a differential target, at a specific location outside the flame, to each differential area on the surface of the flame.

$$F_{dA_t \rightarrow dA_f} = \frac{\cos(\beta_t) \cdot \cos(\beta_f)}{\pi \cdot r^2} \cdot dA_f \quad \text{for } [\beta_t] \text{ and } [\beta_f] < 90^\circ$$

- where: $F_{dA_t \rightarrow dA_f}$ = view factor from a differential area on the target to a differential area on the surface of the flame, dimensionless
 dA_f = differential area on the flame surface, m^2
 dA_t = differential area on the target surface, m^2
 r = distance between differential areas dA_t and dA_f , m
 β_t = angle between normal to dA_t and the line from dA_t to dA_f , degrees
 β_f = angle between normal to dA_f and the line from dA_t to dA_f , degrees

- Step 7: The radiant heat flux incident upon the target is computed by multiplying the view factor for each differential area on the flame by the surface emissive power and by the appropriate atmospheric transmittance, then summing these values over the surface of the flame.

$$q_{ai} = \sum_{A_f} q_{sf} \cdot F_{dA_i \rightarrow dA_f} \cdot \tau$$

where: q_{ai} = attenuated radiant heat flux incident upon the target due to radiant heat emitted by the flame, kW/m²

A_f = area of the surface of the flame

q_{sf} = radiant heat flux emitted by the surface of the flame, kW/m²

τ = atmospheric transmittance, dimensionless

Atmospheric transmittance, τ , is a function of absolute humidity and r , the path length between differential areas on the flame and target [Wayne, 1991].

Step 8: Steps 6 and 7 are repeated for numerous target locations.

Validation

Several of the equations used in the Torch Fire and Flare Radiation Model are empirical relationships based on data from medium- to large-scale experiments, which ensures reasonably good agreement between model predictions and experimental data for variables such as flame tilt angle. Comparisons of experimental data and model predictions for incident heat flux at specific locations are more meaningful and of greater interest. Unfortunately, few reports on medium- or large-scale experiments contain the level of detail required to make such comparisons.

One reasonable source of test data is a report by Chamberlain [1987]. It contains data from seven flare tests involving natural gas releases from industrial flares, with several data points being reported for each test. Variables that were examined during these tests include release diameter (0.203 and 1.07 m), release rate and velocity, and wind speed. Figure C-1 compares the predicted values of incident heat flux with experimental data from the seven flare tests.

References

- Chamberlain, G. A., "Developments in Design Methods for Predicting Thermal Radiation from Flares." *Chemical Engineering Research and Design*, Vol. 65, July, 1987.
- Cook, D. K., M. Fairweather, G. Hankinson, and K. O'Brien, "Flaring of Natural Gas from Inclined Vent Stacks." *ICHEME Symposium Series #102*, Pergamon Press, 1987.
- Kalghatgi, G. T., "The Visible Shape and Size of a Turbulent Hydrocarbon Jet Diffusion Flame in a Cross Wind." *Combustion and Flame*, Vol. 52, 1983: pp. 91-106.
- Wayne, F. D., "An Economical Formula for Calculating Atmospheric Infrared Transmissivities." *Journal of Loss Prevention in the Process Industries*, Vol. 4, January, 1991: pp. 86-92.

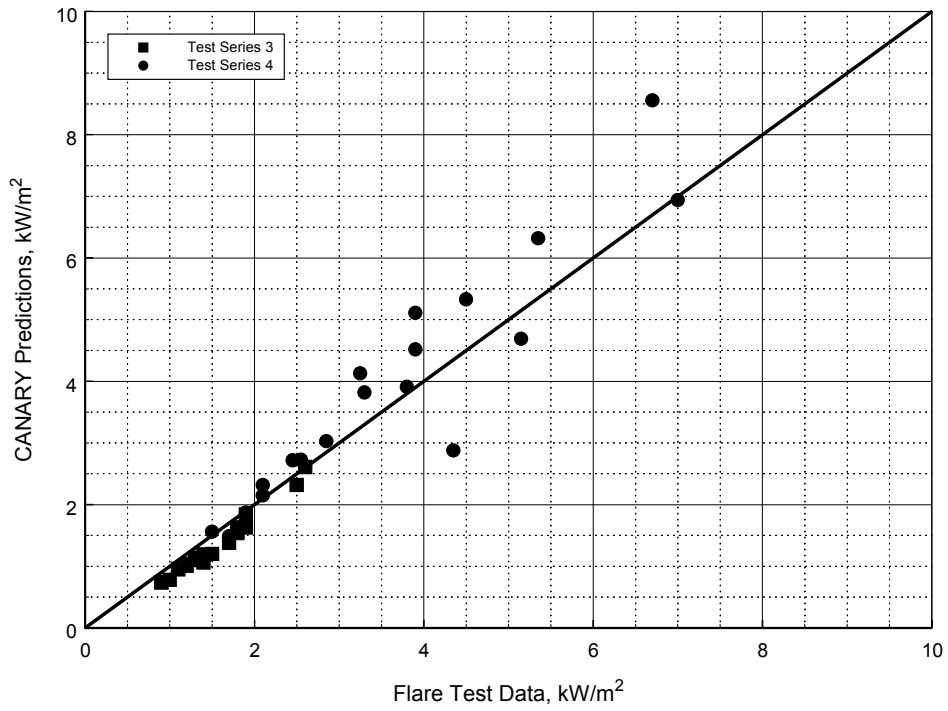


Figure C-1

Fluid Release Model

Purpose

The purpose of the Fluid Release Model is to predict the rate of mass release from a breach of containment. Specifically, the model predicts the rate of flow and the physical state (liquid, two-phase, or gas) of the release of a fluid stream as it enters the atmosphere from a circular breach in a pipe or vessel wall. The model also computes the amount of vapor and aerosol produced and the rate at which liquid reaches the ground.

Required Data

- (a) Composition of the fluid
- (b) Temperature and pressure of the fluid just prior to the time of the breach
- (c) Normal flow rate of fluid into the vessel or in the pipe
- (d) Size of the pipe and/or vessel
- (e) Length of pipe
- (f) Area of the breach
- (g) Angle of release relative to horizontal
- (h) Elevation of release point above grade

Methodology

Step 1: Calculation of Initial Flow Conditions

The initial conditions (before the breach occurs) in the piping and/or vessel are determined from the input data, coupled with a calculation to determine the initial pressure profile in the piping. The pressure profile is computed by dividing the pipe into small incremental lengths and computing the flow conditions stepwise from the vessel to the breach point. As the flow conditions are computed, the time required for a sonic wave to traverse each section is also computed. The flow in any length increment can be all vapor, all liquid, or two-phase (this implies that the sonic velocity within each section may vary). As flow conditions are computed in each length increment, checks are made to determine if the fluid velocity has exceeded the sonic velocity or if the pressure in the flow increment has reached atmospheric. If either condition has been reached, an error code is generated and computations are stopped.

Step 2: Initial Unsteady State Flow Calculations

When a breach occurs in a system with piping, a disturbance in flow and pressure propagates from the breach point at the local sonic velocity of the fluid. During the time required for the disturbance to reach the upstream end of the piping, a period of highly unsteady flow occurs. The portion of the piping that has experienced the passage of the pressure disturbance is in accelerated flow, while the portion upstream of the disturbance is in the same flow regime as before the breach occurred.

To compute the flow rate from the breach during the initial unsteady flow period, a small time increment is selected and the distance that the pressure disturbance has moved in that time increment is computed using the sonic velocity profile found in the initial pressure profile calculation. The

disturbed length is subdivided into small increments for use in an iterative pressure balance calculation. A pressure balance is achieved when a breach pressure is found that balances the flow from the breach and the flow in the disturbed section of piping. Another time increment is added, and the iterative procedure continues. The unsteady period continues until the pressure disturbance reaches the upstream end of the pipe.

Step 3: Long-Term Unsteady State Flow Calculations

The long-term unsteady state flow calculations are characterized by flow in the piping system that is changing more slowly than during the initial unsteady state calculations. The length of accelerated flow in the piping is constant, set by the user input pipe length. The vessel contents are being depleted, resulting in a potential lowering of pressure in the vessel. As with the other flow calculations, the time is incremented and the vessel conditions are computed. The new vessel conditions serve as input for the pressure drop calculations in the pipe. When a breach pressure is computed that balances the breach flow with the flow in the piping, a solution for that time is achieved. The solution continues until the ending time or other ending conditions are reached.

The frictional losses in the piping system are computed using the equation:

$$h = \left(\frac{4 \cdot f \cdot L \cdot U^2}{2 \cdot g_c \cdot D_e} \right) \quad (1)$$

where: h = head (pressure) loss, ft of fluid
 f = friction factor
 L = length of system, ft
 U = average flowing velocity, ft/sec
 g_c = gravitational constant, 32.2 lb_m · ft/(lb_f · sec²)
 D_e = equivalent diameter of duct, ft

The friction factor is computed using the following equation:

$$\frac{1}{\sqrt{f}} = 1.74 - 2.0 \cdot \log_{10} \left[\frac{2 \cdot \varepsilon}{D_e} + \frac{18.7}{Re \cdot \sqrt{f}} \right] \quad (2)$$

where: ε = pipe roughness, ft
 Re = Reynolds number, $D_e \cdot U \cdot \rho / \mu$, dimensionless
 ρ = fluid density, lb/ft³
 μ = fluid viscosity, lb/(ft · sec)

Equations (1) and (2) are used for liquid, vapor, and two-phase flow regimes. Since the piping is subdivided into small lengths, changes in velocity and physical properties across each segment are assumed to be negligible. At each step in the calculation, a check is made to determine if the fluid velocity has reached or exceeded the computed critical (sonic) velocity for the fluid. If the critical velocity has been exceeded, the velocity is constrained to the critical velocity and the maximum mass flow rate in the piping has been set.

If the fluid in the piping is in two-phase flow, the Lockhart and Martinelli [1949] modification to Equation (1) is used. The Lockhart and Martinelli equation for head loss is shown below:

$$h_{TP} = \Phi^2 \cdot \left(\frac{4 \cdot f \cdot L \cdot U_{ls}^2}{2 \cdot g_c \cdot D_e} \right) \quad (3)$$

where: h_{TP} = head loss for two-phase flow, ft of fluid

Φ = empirical parameter correlating single- and two-phase flow, dimensionless

U_{ls} = superficial liquid velocity (velocity of liquid if liquid filled the pipe), ft/sec

This equation is valid over short distances where the flowing velocity does not change appreciably.

Validation

Validation of fluid flow models is difficult since little data are available for comparison. Fletcher [1983] presented a set of data for flashing CFC-11 flowing through orifices and piping. Figures E-1 through E-4 compare calculations made using the Fluid Release Model with the data presented by Fletcher. Figure E-1 compares fluid fluxes for orifice type releases. These releases had length-to-diameter (L/D) ratios less than 0.88. Figure E-2 compares computed and experimental release fluxes for an L/D ratio of 120 at several levels of storage pressure. Figure E-3 compares similar releases for an L/D of 37.5. Figure E-4 shows predicted and experimental release fluxes at a given pressure for L/D ratios from 1 to 200.

Figures E-5 and E-6 compare computed and experimental gas discharge rates for the complete breach of two pipes. One pipe had an internal diameter of 6.2 inches (0.157 m); the other had a diameter of 12 inches (0.305 m). These pipes were initially pressurized to 1,000 psia with air and then explosively ruptured. The experimental values were reported in a research paper for Alberta Environment, authored by Wilson [1981].

Aerosols and Liquid Droplet Evaporation

Liquids stored at temperatures above their atmospheric pressure boiling point (superheated liquids) will give off vapor when released from storage. If the temperature of storage is sufficiently above the normal boiling point, the energy of the released vapor will break the liquid stream into small droplets. If these droplets are small enough, they will not settle, but remain in the vapor stream as aerosol droplets. The presence of aerosol droplets in the vapor stream changes its apparent density and provides an additional source of vapor. Droplets large enough to fall to the ground will lose mass due to evaporation during their fall.

The prediction of aerosol formation and amount of aerosol formed is based on the theoretical work performed for the Center for Chemical Process Safety (CCPS) by CREARE. CREARE's work has been extended and corrected by Quest. The extension to the model computes the non-aerosol drop evaporation. In Figure E-7, the four experimental data sets available for comparison (chlorine (Cl₂), methylamine (MMA), CFC-11, and cyclohexane) are compared to the values computed by the CANARY Aerosol Model.

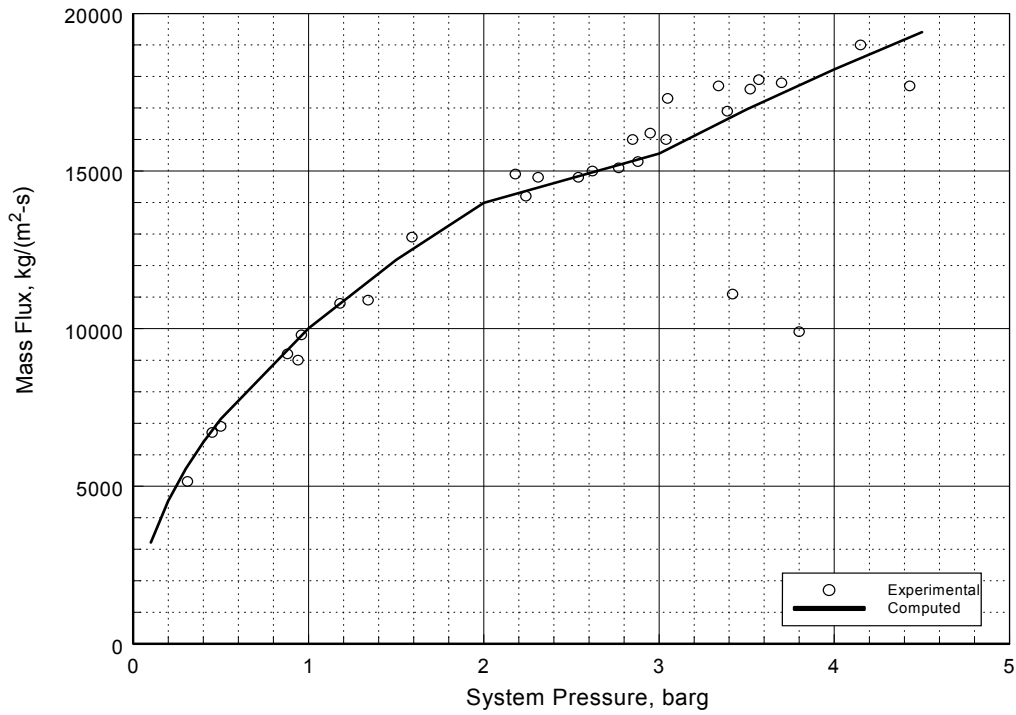


Figure E-1
Comparison of CFC-11 Orifice Releases as a Function of System Pressure

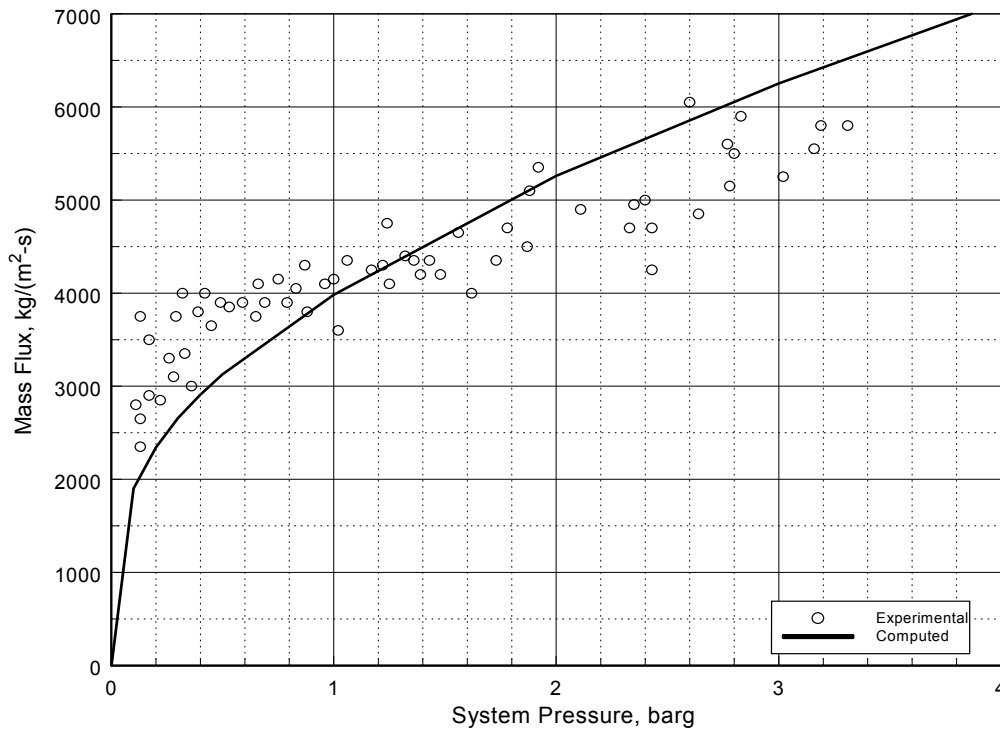


Figure E-2
CFC-11 Release Rate Comparison with L/D of 120

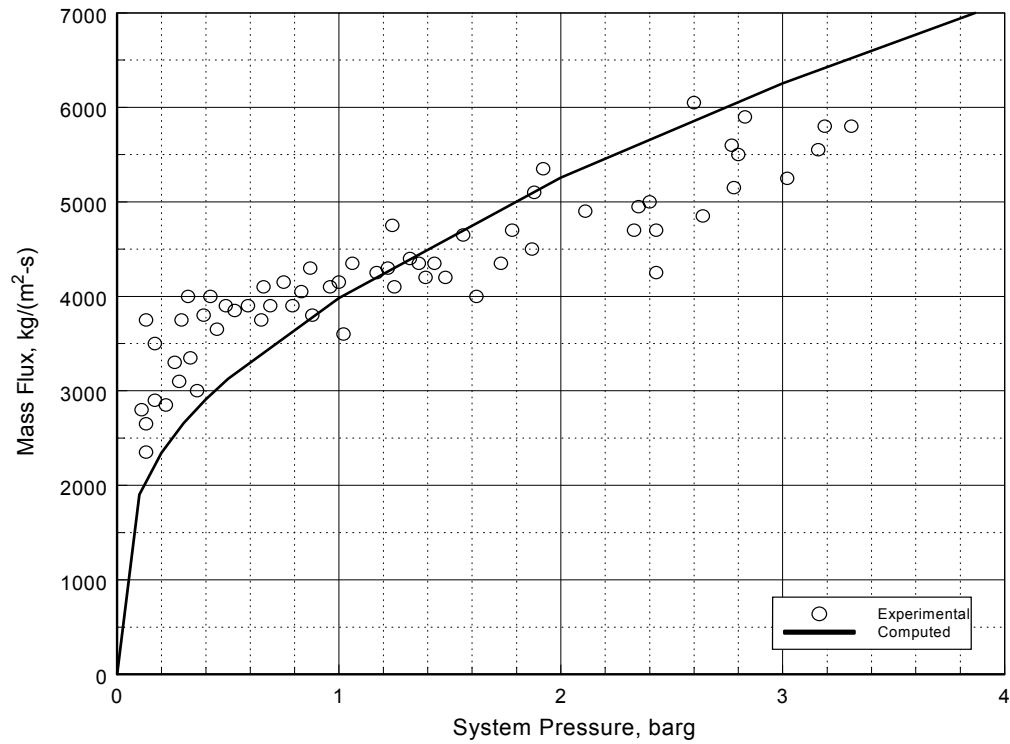


Figure E-3
CFC-11 Release Rate Comparison with L/D of 37.5

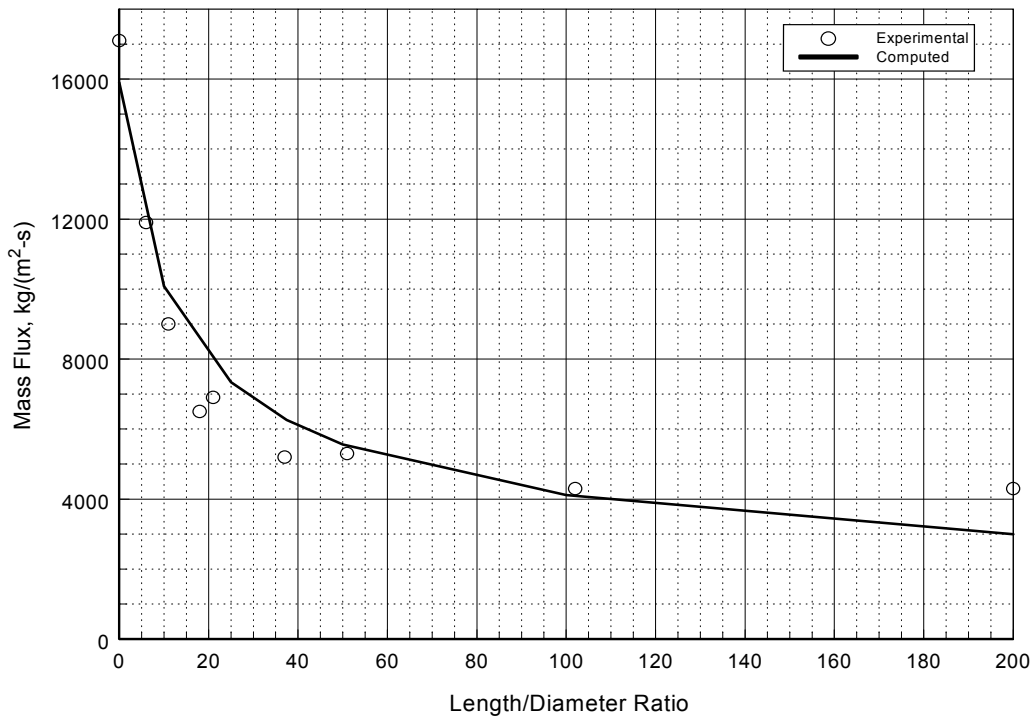


Figure E-4
CFC-11 Release Rate Comparison at Varying L/D Ratios

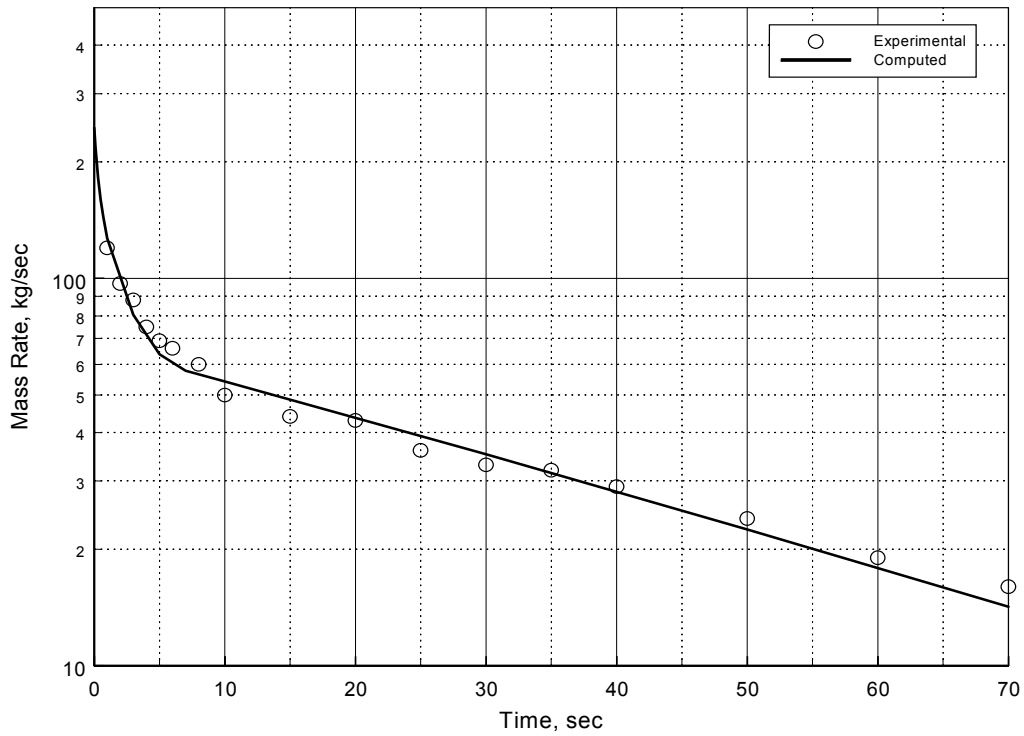


Figure E-5
Air Discharge Rates for 0.157 m Diameter Piping

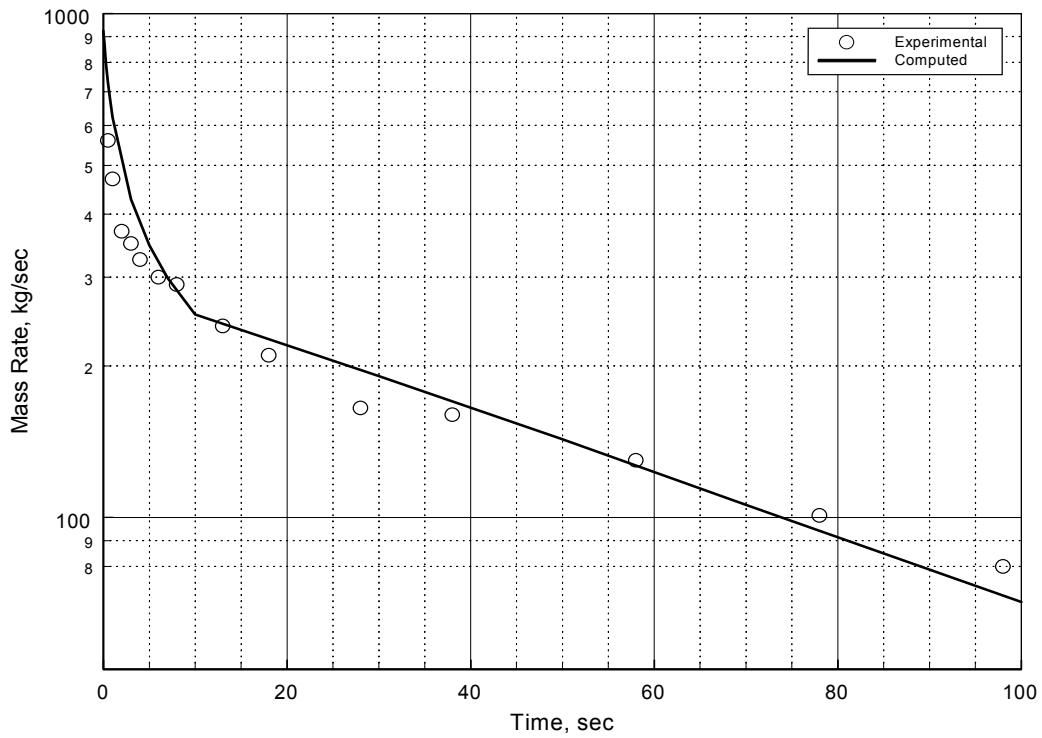


Figure E-6
Air Discharge Rates for 0.305 m Diameter Piping

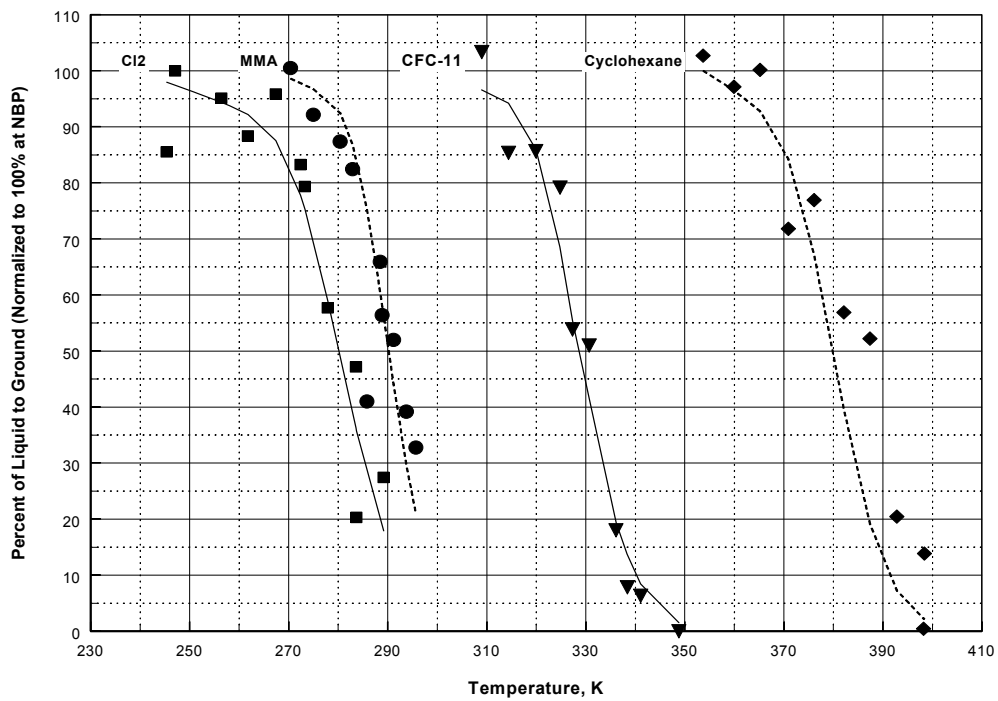


Figure E-7
Aerosol Formation as a Function of Storage Temperature

References

- Fletcher, B., "Flashing Flow Through Orifices and Pipes." Paper presented at the AIChE Loss Prevention Symposium, Denver, Colorado, 1983.
- Lockhart, R. W., and R. C. Martinelli, "Proposed Correlation of Data for Isothermal Two-Phase, Two-Component Flow in Pipes." *Chemical Engineering Progress*, Vol. 45, 1949: p. 39.
- Wilson, D. J., "Expansion and Plume Rise of Gas Jets from High Pressure Pipeline Ruptures." Research Paper, Pollution Control Division, Alberta Environment, April, 1981.

Momentum Jet Dispersion Model

Purpose

The purpose of this model is to predict the dispersion of a jet release into ambient air. It is used to predict the downwind travel of a flammable or toxic gas or aerosol momentum jet release.

Required Data

- (a) Composition and properties of the released material
- (b) Temperature of released material
- (c) Release rate of material
- (d) Vertical release angle relative to wind direction
- (e) Height of release
- (f) Release area
- (g) Ambient wind speed
- (h) Ambient Pasquill-Gifford stability class
- (i) Ambient temperature
- (j) Relative humidity
- (k) Surface roughness scale

Methodology

Step 1: An assumption is made that flow perpendicular to the main flow in the plume is negligible, that the velocity and concentration profiles in the jet are similar at all sections of the jet, that molecular transport in the jet is negligible, and that longitudinal turbulent transport is negligible when compared to longitudinal convective transport. The coordinate system is then defined in s and r , where s is the path length of the plume and r is the radial distance from the plume centerline. The angle between the plume axis and horizontal is referred to as θ . Relationships between the downwind coordinate, x , vertical coordinate, y , and plume axis are given simply by:

$$\frac{dx}{ds} = \cos(\theta) \quad (1)$$

and

$$\frac{dy}{ds} = \sin(\theta) \quad (2)$$

Step 2: Velocity, concentration, and density profiles are assumed to be cylindrically symmetric about the plume axis and are assumed to be Gaussian in shape. The three profiles are taken as:

$$u(s, r, \theta) = U_a \cdot \cos(\theta) + u^*(s) \cdot e^{\frac{-r^2}{b^2(s)}} \quad (3)$$

where: u = plume velocity, m/s
 U_a = ambient wind speed, m/s
 u^* = plume velocity relative to the wind in the downwind direction at the plume axis, m/s
 $b(s)$ = characteristic width of the plume at distance s from the release, m

$$\rho(s, r, \theta) = \rho_a + \rho^*(s) \cdot e^{\frac{-r^2}{\lambda^2 \cdot b^2(s)}} \quad (4)$$

where: ρ = plume density, kg/m³
 ρ_a = density of ambient air, kg/m³
 $\rho^*(s)$ = density difference between plume axis and ambient air, kg/m³
 λ^2 = turbulent Schmidt number, 1.35

$$c(s, r, \theta) = c^*(s) \cdot e^{\frac{-r^2}{\lambda^2 \cdot b^2(s)}} \quad (5)$$

where: c = pollutant concentration in the plume, kg/m³
 $c^*(s)$ = pollutant concentration at plume centerline, kg/m³

Step 3: The equation for air entrainment into the plume and the conservation equations can then be solved. The equation for air entrainment is:

$$\begin{aligned} \frac{d}{ds} \left(\int_0^{b\sqrt{2}} \rho \cdot u \cdot 2 \cdot \pi \cdot dr \right) \\ = 2 \cdot \pi \cdot b \cdot \rho_a \cdot \left\{ \alpha_1 \cdot |u^*(s)| + \alpha_2 \cdot U_a \cdot |\sin(\theta)| \cos(\theta) + \alpha_3 \cdot u' \right\} \end{aligned} \quad (6)$$

where: α_1 = entrainment coefficient for a free jet, 0.057
 α_2 = entrainment coefficient for a line thermal, 0.5
 α_3 = entrainment coefficient due to turbulence, 1.0
 u' = turbulent entrainment velocity (root mean square of the wind velocity fluctuation is used for this number), m/s

Step 4: The equations of conservation of mass, momentum, and energy are given as:

$$\frac{d}{ds} \left(\int_0^{b\sqrt{2}} c \cdot u \cdot 2 \cdot \pi \cdot dr \right) = 0 \quad (7)$$

$$\begin{aligned} \frac{d}{ds} \left(\int_0^{b\sqrt{2}} (\rho \cdot u^2 \cdot \cos(\theta)) \cdot 2 \cdot \pi \cdot dr \right) \\ = 2 \cdot \pi \cdot b \cdot \rho_a \cdot \left\{ \alpha_1 \cdot |u^*(s)| + \alpha_2 \cdot U_a \cdot |\sin(\theta)| \cdot \cos(\theta) + \alpha_3 \cdot u' \right\} \\ + C_d \cdot \pi \cdot b \cdot \rho_a \cdot U_a^2 |\sin(\theta)| \end{aligned} \quad (8)$$

$$\begin{aligned} \frac{d}{ds} \left(\int_0^{b\sqrt{2}} \rho \cdot u^2 \cdot \cos(\theta) \cdot 2 \cdot \pi \cdot dr \right) & \quad (9) \\ & = \int_0^{b\sqrt{2}} g \cdot (\rho_a - \rho) \pi \cdot r \cdot dr \pm C_d \cdot \pi \cdot b \cdot \rho_a \cdot U_a^2 \cdot \sin(\theta) \cdot \cos(\theta) \end{aligned}$$

$$\begin{aligned} \frac{d}{ds} \left(\int_0^{b\sqrt{2}} \rho \cdot u \left(\frac{1}{\rho} - \frac{1}{\rho_{a0}} \right) \cdot 2 \cdot \pi \cdot r \cdot dr \right) & \quad (10) \\ & = \rho_a \cdot 2 \cdot \pi \cdot b \left(\frac{1}{\rho_a} - \frac{1}{\rho_{a0}} \right) \cdot \left\{ \alpha_1 \cdot |u^*(s)| + \alpha_2 \cdot U_a \sin(\theta) \cdot \cos(\theta) + \alpha_3 \cdot \dot{u} \right\} \end{aligned}$$

The subscript 0 refers to conditions at the point of release. These equations are integrated along the path of the plume to yield the concentration profiles as a function of elevation and distance downwind of the release.

Step 5: After the steady-state equations are solved, an along-wind dispersion correction is applied to account for short-duration releases. This is accomplished using the method outlined by Palazzi, et al. [1982].

Step 6: If the plume reaches the ground, it is coupled to the Heavy Gas Dispersion Model (described in Section G) and the dispersion calculations continue.

Validation

The Momentum Jet Dispersion Model used in CANARY was validated by comparing results obtained from the model with experimental data from field tests. Data used for this comparison and the conditions used in the model were taken from an American Petroleum Institute (API) study [Hanna, Strimaitis, and Chang, 1991]. For this model, comparisons were made with the Desert Tortoise, Goldfish, and Prairie Grass series of dispersion tests. Results of these comparisons are shown in Figure F-1.

References

- Astleford, W. J., T. B. Morrow, and J. C. Buckingham, *Hazardous Chemical Vapor Handbook for Marine Tank Vessels* (Final Report – Phase II). U.S. Coast Guard Report No. CG-D-12-83, April, 1983.
- Hanna, S. R., D. G. Strimaitis, and J. C. Chang, *Hazard Response Modeling Uncertainty (A Quantitative Method), Evaluation of Commonly Used Hazardous Gas Dispersion Models*, Volume II. Study co-sponsored by the Air Force Engineering and Services Center, Tyndall Air Force Base, Florida, and the American Petroleum Institute; performed by Sigma Research Corporation, Westford, Massachusetts, September, 1991.
- Havens, J., and T. Spicer, *LNG Vapor Dispersion Prediction with the DEGADIS Dense Gas Dispersion Model*. Gas Research Institute Contract No. 5086-252-1287 with the University of Arkansas, September, 1990: pp. 37-48.
- Ooms, G., "A New Method for the Calculation of the Plume Path of Gases Emitted by a Stack." *Atmospheric Environment*, Vol. 6, 1972: pp. 889-909.

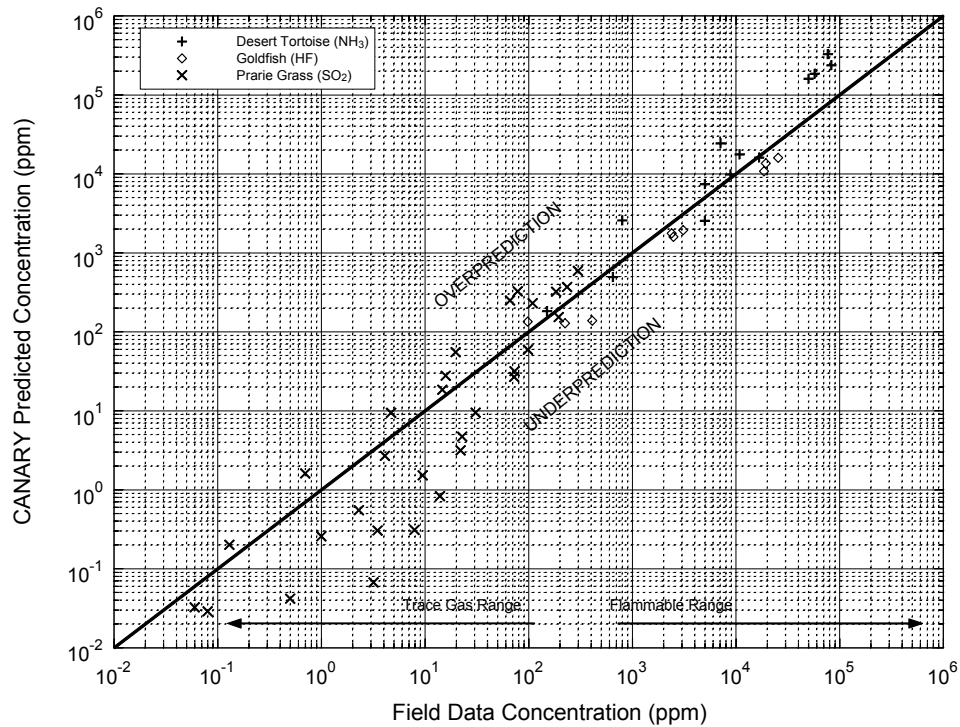


Figure F-1

Ooms, G., A. P. Mahieu, and F. Zelis, "The Plume Path of Vent Gases Heavier than Air." *First International Symposium on Loss Prevention and Safety Promotion in the Process Industries*, C. H. Buschman, Editor, Elsevier Press, 1974.

Palazzi, E., M. De Faveri, G. Fumarola, and G. Ferraiolo, "Diffusion from a Steady Source of Short Duration." *Atmospheric Environment*, Vol. 16, No. 12, 1982: pp. 2785-2790.

Heavy Gas Dispersion Model

Purpose

The purpose of this model is to predict the dispersion and gravity flow of a heavy gas released into the air from liquid pools or instantaneous gas releases. It is used to predict the downwind travel of a flammable or toxic vapor cloud.

Required Data

- (a) Composition and properties of the released material
- (b) Temperature of released material
- (c) Vapor generation rate
- (d) Vapor source area
- (e) Vapor source duration
- (f) Ambient wind speed
- (g) Ambient Pasquill-Gifford atmospheric stability class
- (h) Ambient temperature
- (i) Relative humidity
- (j) Surface roughness scale

Methodology

Step 1: For a steady-state plume, released from a stationary source, the Heavy Gas Dispersion Model solves the following equations:

$$\frac{d}{dx}(\rho \cdot U \cdot B \cdot h \cdot m) = \rho_s \cdot W_s \cdot B_s \quad (1)$$

$$\frac{d}{dx}(\rho \cdot U \cdot B \cdot h) = \rho_a \cdot (V_e \cdot h + W_e \cdot B) + \rho_s \cdot W_s \cdot B_s \quad (2)$$

$$\frac{d}{dx}(\rho \cdot U \cdot B \cdot h \cdot C_p \cdot T) = \rho_a \cdot (V_e \cdot h + W_e \cdot B) \cdot C_{pa} \cdot T_a + \rho_s \cdot W_s \cdot B_s \cdot C_{ps} \cdot T_s + f_t \quad (3)$$

$$\begin{aligned} \frac{d}{dx}(\rho \cdot U \cdot B \cdot h \cdot U) \\ = -0.5 \cdot \alpha_g \cdot g \cdot \frac{d}{dx}[(\rho - \rho_a) \cdot B \cdot h^2] + \rho_a \cdot (V_e \cdot h + W_e \cdot B) \cdot U_a + f_u \end{aligned} \quad (4)$$

$$\frac{d}{dx}(\rho \cdot U \cdot B \cdot h \cdot V_g) = g \cdot (\rho - \rho_a) \cdot h^2 + f_{vg} \quad (5)$$

$$U \cdot \frac{dZ_c}{dx} = -V_g \cdot \frac{Z_c}{B} \quad (6)$$

$$U \cdot \frac{dB}{dx} = \frac{\rho_a}{\rho} \cdot V_e + V_g \quad (7)$$

$$\rho \cdot T = \frac{\rho_a \cdot T_a \cdot M_s}{[M_s + (M_a - M_s) \cdot m]} \quad (8)$$

where: x = downwind distance, m
 ρ = density, kg/m³
 U = velocity in the direction of the wind, m/s
 B = cloud width parameter, m
 h = cloud height parameter, m
 m = mass fraction of source gas
 T = temperature, K
 C_p = specific heat, J/(kgⓈ)
 f_t = ground heat flux, J/(mⓈ)
 f_u = downwind friction term, kg/s²
 f_v = crosswind friction term, kg/s²
 V_e = horizontal entrainment rate, m/s
 V_g = horizontal crosswind gravity flow velocity, m/s
 W_e = vertical entrainment rate, m/s
 W_s = vertical source gas injection velocity, m/s
 M = molecular weight, kg/kmole
 s = refers to source properties
 a = refers to ambient properties

The first six equations are crosswind-averaged conservation equations. Equation (7) is the width equation, and Equation (8) is the equation of state.

Step 2: All of the gas cloud properties are crosswind averaged. The three-dimensional concentration distribution is calculated from the average mass concentration by assuming the following concentration profile:

$$C(x, y, z) = C(x) \cdot C_1(y) \cdot C_2(z) \quad (9)$$

$$C(x) = \frac{M_a \cdot m(x)}{M_s + (M_a - M_s) \cdot m(x)} \quad (10)$$

$$C_1(y) = \frac{1}{4 \cdot b} \cdot \left\{ \operatorname{erf} \left(\frac{y+b}{2 \cdot \beta} \right) - \operatorname{erf} \left(\frac{y-b}{2 \cdot \beta} \right) \right\} \quad (11)$$

$$B^2 = b^2 + 3 \cdot \beta^2 \quad (12)$$

$$C_2(z) = \left(\frac{6}{\pi}\right)^{1/2} \cdot \frac{1}{h} \cdot \exp\left(\frac{-3 \cdot z^2}{2 \cdot h^2}\right) \quad (13)$$

where: $C(x, y, z)$ = concentration in plume at x, y, z , kg/m³
 y = crosswind coordinate, m
 z = vertical coordinate, m
 b, B, β = half-width parameters, m

Step 3: As there are now two parameters used to define $C_1(y)$, the following equation is needed to calculate b :

$$U \cdot \left(\frac{db}{dx}\right) = V_g \cdot \frac{b}{B} \quad (14)$$

Step 4: The vertical entrainment rate is defined to be:

$$W_e = \frac{\sqrt{3} \cdot a \cdot k \cdot U_* \cdot \delta\left(\frac{h}{H}\right)}{\Phi_h\left(\frac{h}{L}\right)} \quad (15)$$

where: a = constant, 1.5
 k = constant, 0.41
 U_* = friction velocity, m/s
 L = Monin-Obukhov length derived from the atmospheric stability class

Step 5: The profile function δ is used to account for the height of the mixing layer, H , and to restrict the growth of the cloud height to that of the mixing layer. H is a function of stability class and is defined as:

$$\delta\left(\frac{h}{H}\right) = 1 - \frac{h}{H} \quad (16)$$

The Monin-Obukhov function, Φ_h , is defined by:

$$\Phi_h\left(\frac{h}{L}\right) = \begin{cases} 1 + 5 \cdot \frac{h}{L} & L \geq 0 \text{ (stable)} \\ \left[1 - 16 \cdot \frac{h}{L}\right]^{-1/2} & L < 0 \text{ (unstable)} \end{cases} \quad (17)$$

Step 6: After the steady-state equations are solved, an along-wind dispersion correction is applied to account for short-duration releases. This is accomplished using the method outlined by Palazzi, et al. [1982].

Validation

The Heavy Gas Dispersion Model used in CANARY was validated by comparing results obtained from the model with experimental data from field tests. Data used for this comparison and the conditions used in the model were taken from an American Petroleum Institute (API) study [Hanna, Strimaitis, and Chang, 1991]. For this model, comparisons were made with the Burro, Maplin Sands, and Coyote series of dispersion tests. Results of these comparisons are shown in Figure G-1.

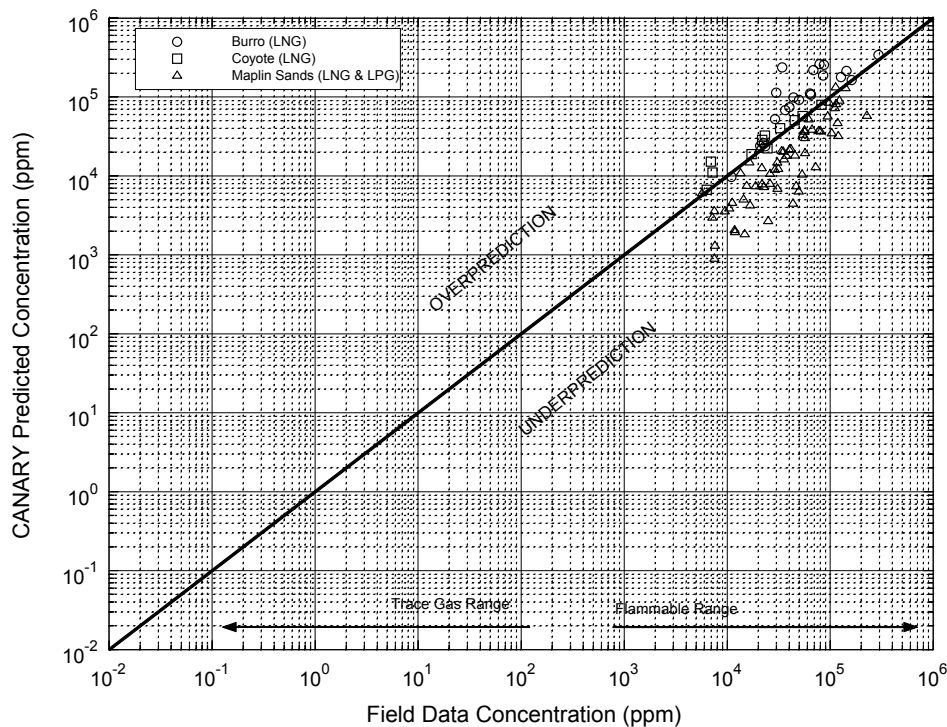


Figure G-1

References

- Ermak, D. L., and S. T. Chan, *A Study of Heavy Gas Effects on the Atmospheric Dispersion of Dense Gases*. UCRL-92494, Lawrence Livermore National Laboratory, Livermore, California. Presented at the 15th NATO/CCMS International Technical Meeting on Air Pollution Modeling and Its Applications, St. Louis, Missouri, April 15-19, 1985.
- Ermak, D. L., S. T. Chan, D. L. Morgan, Jr., and L. K. Morris, "A Comparison of Dense Gas Dispersion Model Simulations with Burro Series LNG Spill Test Results." *Journal of Hazardous Materials*, Vol. 6, 1982: pp. 129-160.
- Ermak, D. L., and S. T. Chan, *Recent Developments on the FEM3 and SLAB Atmospheric Dispersion Models*. UCRL-94071, Lawrence Livermore National Laboratory, Livermore, California. Presented at the IMA Conference on Stably Stratified Flows and Dense Gas Dispersion, Chester, England, April 9-10, 1986.
- Hanna, S. R., D. G. Strimaitis, and J. C. Chang, *Hazard Response Modeling Uncertainty (A Quantitative Method)*, *Evaluation of Commonly-Used Hazardous Gas Dispersion Models*, Volume II. Study cosponsored by the Air Force Engineering and Services Center, Tyndall Air Force Base, Florida, and the

American Petroleum Institute; performed by Sigma Research Corporation, Westford, Massachusetts, September, 1991.

Morgan, D. L., L. K. Morris, S. T. Chan, D. L. Ermak, T. G. McRae, R. T. Cederwall, R. P. Kooperman, H. C. Goldwire, Jr., J. W. McClure, and W. J. Hogan, *Phenomenology and Modeling of Liquefied Natural Gas Vapor Dispersion*. UCRL-53581, Lawrence Livermore National Laboratory, Livermore, California, 1982.

Morgan, D. L., Jr., L. K. Morris, and D. L. Ermak, *SLAB: A Time-Dependent Computer Model for the Dispersion of Heavy Gases Released in the Atmosphere*. UCRL-53383, Lawrence Livermore National Laboratory, Livermore, California, 1983.

Palazzi, E., M. De Faveri, G. Fumarola, and G. Ferraiolo, "Diffusion from a Steady Source of Short Duration." *Atmospheric Environment*, Vol. 16, No. 12, 1982: pp. 2785-2790.